On the accuracy of predicting shear viscosity of molecular liquids using the periodic perturbation method

Lifeng Zhao, Tao Cheng, and Huai Sun[a)]
School of Chemistry and Chemical Technology, Shanghai Jiao Tong University, Shanghai 200240, China

(Received 24 December 2007; accepted 6 May 2008; published online 8 October 2008)

Non-equilibrium molecular dynamics simulations are performed to calculate shear viscosities of 16 representative molecular liquids using the periodic perturbation method (PPM). A perturbation index is defined to measure the strength of the perturbation. It is identified that the predictions are systematically underestimated using PPM. The origin of the underestimate is the acoustic wave in the liquid density, which is persistent in the simulation box unless the perturbation is completely removed. However, there is a linear correlation between the perturbation indexes and the apparent viscosities, which can be utilized to accurately predict the shear viscosities. Finally, it is demonstrated that general force fields derived based on equilibrium properties can be used to predict the shear viscosities of small molecular liquids with relative errors less than 10%. © *2008 American Institute of Physics*. [DOI: 10.1063/1.2936986]

I. INTRODUCTION

As one of the most important transport properties, shear viscosity has been a focus of prediction using computer simulations for years. Methods using equilibrium molecular dynamics are based on the fluctuation theorem. Either pressure fluctuation[1] or momentum fluctuation[2] can be used to calculate the shear viscosity. Because of heavy fluctuation and low signal-to-noise ratio, the efficiency has been an issue of concern.[3] From the 1970s, several methods based on non-equilibrium molecular dynamics simulations have been developed for calculating the shear viscosities. The SLLOD algorithm[4] estimates the viscosity by imposing a linear velocity profile in the simulation box. The periodic perturbation method (PPM)[5,6] is based on the same theoretical foundation as the momentum fluctuations method; however, instead of measuring the intrinsic fluctuations of momentum, an external force profile is applied to the simulation box and the viscosity is measured from the fluctuations of the induced momentums. Consequently, the signal-to-noise ratio is enhanced, which leads to better statistics of the calculated results. Other methods available include the reversed flux-velocity profile method[7] and the momentum impulse relaxation (MIR) method.[8]

The PPM has been applied in a few systems. Vasquez[9] applied the PPM to Lennard-Jones liquid with a range of acceleration amplitudes. Hess[10] has compared the PPM with several EMD and NEMD methods with Lennard-Jones liquid and SPC water. Wensink *et al.*[11] applied the PPM to water/alcohol mixtures. Recently our group calculated the shear viscosities of several alcohol molecules at two state points of (373 K, 0.1 MPa) and (373 K, 250 MPa) with the PPM.[12] In our work, it was found that the calculated viscosities are linearly and negatively correlated with the applied external force strength (the acceleration amplitude) and the "zero perturbed" viscosity values can be obtained by lineally extrapolating the data. This finding is contradictory with what has been reported in the literature using the same[9,10] and other[4] perturbation methods. It was generally suggested that a plateau should be reached as the acceleration amplitude was gradually reduced and the "true" value could be obtained at the plateau. Therefore, a question needs to be addressed. Is the linear and negative dependence of the calculated viscosities with respect to the acceleration amplitudes as we observed generally true? In order to answer this question, we need to find out the origin of the correlation and the factors that make the influences. In addition, we want to see if this method can be extended to predict shear viscosities of molecular liquids using a general force field such as OPLS.[13] Since general force field parameters are derived only based on equilibrium properties, it is unclear if they can be used to predict the transport properties accurately. These questions motivated the present study.

II. METHOD

The PPM is well explained in the literature by Hess.[10] For the completeness of information a short summary is given here.

The simulations are carried out in 3-D periodic cells in a way similar to normal molecular dynamics simulations. During the simulation, a periodic external force $\mathbf{a}(z)$, which is a function of the z-direction coordinate, is applied in the x-direction to each of the particles. Consequently, a velocity field $\mathbf{u}$ of the fluid is created. The velocity field $\mathbf{u}$ satisfies the Navier-Stokes equation:[1]

$$\rho\frac{\partial \mathbf{u}}{\partial t} + \rho(\mathbf{u}\cdot\nabla)\mathbf{u} = \rho\mathbf{a} - \nabla p + \eta\nabla^2\mathbf{u}. \quad (1)$$

Since u_y and u_z are zeros, and there is no pressure gradient in the x-direction, the equation is simplified to

[a)]Author to whom correspondence should be addressed. Telephone: +86-21-5474-8987; Fax: +86-21-5474-1297. Electronic mail: huaisun@sjtu.edu.cn.

TABLE I. Molecular liquids investigated in this work. The number of molecules N_{mol}, cell edge l_z (in nm), and temperature T (in Kelvin) are listed. The pressure is at 1 atm for all liquid.

Molecule	N_{mol}	T	l_z
Acetone	400	298	3.625
Benzene	360	298	3.770
Ether	320	273	3.758
Heptane	230	298	3.837
Toluene	360	298	3.993
Propene	500	200	3.762
Cresol	320	353	3.868
Ethylacetate	360	298	3.859
Isobutane	230	223	3.222
Cyclohexane	270	298	3.693
Formic acid	729	298	3.572
Butane	230	223	3.228
Pentane	300	277	3.823
Decane	216	293	4.122
Hexane	170	298	3.223
Ethanol	240	298	2.874

$$\rho\frac{\partial u_x(z)}{\partial t} = \rho a_x(z) + \eta\frac{\partial^2 u_x(z)}{\partial z^2}. \tag{2}$$

The steady-state is given by

$$a_x(z) + \frac{\eta}{\rho}\frac{\partial^2 u_x(z)}{\partial z^2} = 0. \tag{3}$$

The periodic force can be realized by applying an acceleration profile:

$$a_x(z) = \Lambda\cos(kz), \tag{4}$$

where Λ is the acceleration amplitude, which specifies the magnitude of the force applied. The wave vector is defined as

$$k = 2\pi/l_z, \tag{5}$$

where l_z is the length of the box in the z-direction.

With the applied acceleration (force), a generated velocity profile is given as

$$u_x(z,t) = V(1 - e^{-t/\tau_r})\cos(kz), \tag{6}$$

$$V = \frac{\Lambda}{\eta}\frac{\rho}{k^2}, \tag{7}$$

where τ_r is given by

$$\tau_r = \frac{\rho}{\eta k^2}. \tag{8}$$

When $t \gg \tau_r$, the velocity profile is fully developed and time independent:

$$u_x(z) = V\cos(kz). \tag{9}$$

Therefore, by measuring the quantity V the viscosity can be derived using Eq. (7).

In order to calculate the quantity V, multiply both sides of Eq. (9) by $\cos(kz)$ and integrate the resulting equation; one then has

$$V = \frac{2}{l_z}\int_0^{l_z} u_x(z)\cos(kz)dz. \tag{10}$$

Since $u_x(z)$ in Eq. (10) is the velocity of an infinitesimal mass, the integration (10) is written into numerical summation of data taken from MD simulation trajectories. At any given time t,

$$V(t) = 2\sum_{i=1}^{N} m_i v_{i,x}(t)\cos(kr_{i,z}(t))/\sum_{i=1}^{N} m_i. \tag{11}$$

The $v_{i,x}(t)$ is the x-direction velocity of atom i at time t. The quantity V is obtained by averaging $V(t)$ over the time of simulation.

From the above deduction, it is clear that the calculated viscosity depends on the acceleration amplitude Λ in a complex way. According to Eq. (7) the value of Λ is proportional to the viscosity η. However, the Λ regulates the value of V, which is reversely proportional to the viscosity η. Generally speaking, the acceleration amplitude should be small enough so that the perturbation does not disturb the equilibrium of the system. On the other hand, the small force leads to low signal-to-noise ratio.

In this work, the MD simulations were performed with cubic periodic boundary conditions. The cell edges ranged from 3.0 to 4.0 nm. The simulations were generally carried out in NPT ensemble; the NVT ensemble was used for analysis purposes. The Berendsen barostat and Berendsen thermostat were used for pressure and temperature controls. The electrostatic energy was integrated using the particle-mesh Ewald (PME) method, with cutoff value of 1.0 nm and relative accuracy of direct-part Ewald potential of 10^{-5} at the cutoff. The van der Waals interactions were evaluated with 1.1 nm cutoff plus tail corrections. The nonbond neighbor list was updated every five steps. In most cases, the equilibration period was at least 0.5 ns, and the data collection period was 1.0 ns. The time step used was normally 1.0 fs, except that a 2.0 fs time step was used for liquid argon. The instantaneous velocities [Eq. (9)] were evaluated in an interval of 0.1 ps from the trajectory.

The uncertainties of the predicted values were estimated using the blocking average method.[14] In this method, the standard deviation of variable x_k measured using a block size of m data points is calculated by

$$\sigma(m) \approx \sqrt{\frac{c_0(n/m)}{n/m-1}}\left(1 \pm \frac{1}{\sqrt{2(n/m-1)}}\right), \tag{12}$$

where n is number of total data points, and $c_0(n/m)$ is defined as

$$c_0(t) = \frac{1}{t}\sum_{k=1}^{t}(x_k - \bar{x})^2. \tag{13}$$

Generally speaking, $\sigma(m)$ varies as the block size m increases. As the size m reaches a certain point, the calculated $\sigma(m)$ value converges. The plateau corresponds to the estimated uncertainty.

The block size measures the time of correlation in the measurements. In this work, we found the correlation times

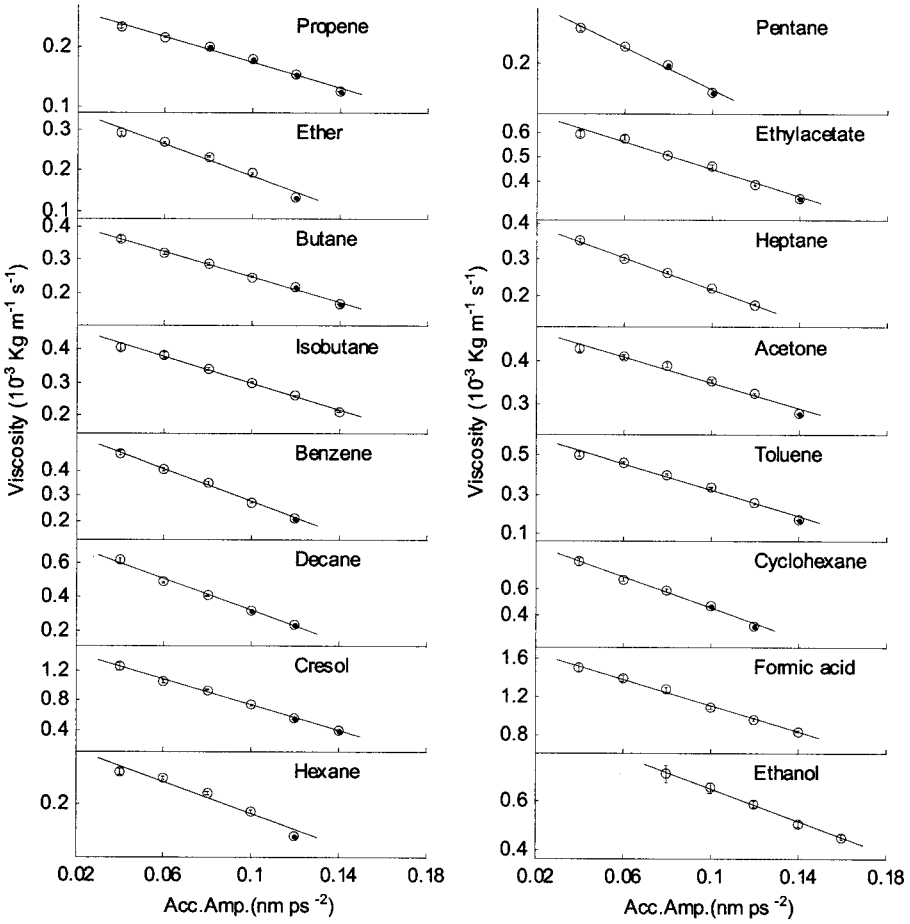

FIG. 1. The shear viscosities calculated at various applied acceleration amplitudes (Λ) for 16 molecular liquids. The straight lines are obtained by least square fit of the calculated data.

range from 0.8 to 3 ps and they are relevant to applied acceleration amplitudes. The larger the acceleration amplitude, the longer the correlation time is.

In order to test if the method and underlying force field are generally applicable, 16 molecular liquids were calculated in this work (see Table I). These molecules are representatives of polar, nonpolar, and aromatic molecules. The OPLS-AA force field was used for these molecules. In addition, liquid argon was used for analysis. The force field parameters for argon are taken from the literature.[15] Molecular dynamics simulations were carried out using GROMACS 3.3.1 software package.[16]

III. RESULTS AND DISCUSSIONS

First of all, we noticed that there is no plateau in the curve of the calculated viscosity as the acceleration amplitudes of the applied external forces change. This is clearly shown in Fig. 1 where the calculated shear viscosities of the 16 molecular liquids with various acceleration amplitudes are plotted. The simulations were conducted at 1 atm pressure; the temperatures and box sizes of the simulations are listed in Table I. Overall, the calculated values are lower than the corresponding experimental data and they are negatively correlated with the acceleration amplitude. Moreover, each of the predictions can be nicely represented by fitting to a straight line. As the applied acceleration amplitudes continue to increase, we found the calculated viscosity values may go upward after a minimum is reached or the simulation may become unstable due to the large perturbation. For all of the 16 molecular liquids, we did not obtain a stable plateau.

This finding is different from what has been reported in the literature.[9,10] For example, Vasquez *et al.*[9] reported a stable region where the calculated viscosity does not change significantly with changes in the value of the acceleration amplitude and used the region to estimate the shear viscosity. These authors discarded the calculated viscosities at low values of the external forces because the data were associated with very large uncertainties. This may be related to the system studied (LJ liquid) being too simple and the simulation variables that can significantly influence the results were not completely sorted out. What we have found (as given in Fig. 1) is that reliable results with acceptable uncertainties can be obtained consistently at the region of much weaker perturbation forces than those used in the work reported previously.[9] This is feasible only with carefully optimized simulation conditions that are to be addressed in this paper.

A. Measurement of the perturbation strength

In order to understand the phenomenon of the underestimate, we studied how the simulation options influence the predictions. We used two systems, liquid argon at 86.0 K and liquid ethanol at 298 K, both under 1 atm, as test cases. The force fields have been well established and validated for both systems.[12,17]

TABLE II. Calculated viscosities η (in 10^{-3} kg m^{-1} s^{-1}) of liquid argon and ethanol with various periodic wavelengths l_z (in nm). The applied acceleration amplitude is 0.01 nm ps^{-2} for argon and 0.1 nm ps^{-2} for ethanol.

	l_z	η
Argon	3.62	0.252 ± 0.004
	7.24	0.237 ± 0.001
	10.86	0.196 ± 0.001
Ethanol	2.80	0.783 ± 0.022
	5.60	0.617 ± 0.006

The size of the k-vector, which is inverse-proportional to the wavelength (l_z) of the periodic perturbation [Eq. (5)], should be set small enough in order to use the Navier-Stokes equation. Hess[10] suggested that the wavelength (l_z) should be at least one magnitude larger than the size of the molecule. The influence of extended wavelengths was investigated using liquid argon and liquid ethanol in this work. The simulations were performed using NVT ensemble. Two wavelengths of 2.8 and 5.6 nm were used for liquid ethanol and three wavelengths of 3.62, 7.24, and 10.86 nm were used for liquid argon. The applied acceleration amplitudes are 0.1 nm ps^{-2} for ethanol and 0.01 nm ps^{-2} for liquid argon. Smaller acceleration amplitude is required for liquid argon because the intermolecular interaction is much weaker in liquid argon than that in liquid ethanol. The calculated viscosity values are listed in Table II. It is clear that the calculated viscosity decreases as the wavelength increases and, even with very large wavelengths, the results appear to have no sign of convergence. This is contradictory with the general statement that the k-vector should be extrapolated to zero to get the accurate prediction of shear viscosity.[18]

Another critical factor that must be considered is the acceleration amplitude Λ. As shown in Fig. 2, the calculated viscosities with different values of Λ are plotted for both liquid argon (a) and ethanol (b). The predicted viscosities are correlated with the applied forces. Generally speaking, as the acceleration amplitude Λ increases, the calculated viscosity decreases. In the range of acceleration amplitude Λ considered, there is a linear relationship between the applied force and the calculated viscosity. In addition, the uncertainty of the prediction increases as the acceleration amplitude Λ decreases, which is clearly demonstrated by the calculated error-bars in the ethanol case [Fig. 2(b)]. For liquid ethanol, results obtained with different perturbation wavelengths (the cell edges in the z-direction) are given. It should be noted that the linear response region is correlated with the perturbation wavelengths. With greater wavelength (l_z=5.6) the applicable acceleration amplitudes Λ are generally smaller than those with smaller wavelength (l_z=2.8). The predicted shear viscosities are generally lower than the experimental value for any applied acceleration amplitudes. However, the data can be well represented by straight lines, and the lines converge to the experimental data,[19,20] which are denoted by dots in the figure.

If the simulations are performed with NVT ensemble, the deviation of the system pressure from its equilibrium value is an indicator of the strength of the perturbation. We found that the system pressures are correlated with the perturbation wavelengths and the acceleration amplitudes in the NVT simulations. With fixed k value, the system pressure increases as the applied acceleration amplitude increases. At fixed acceleration amplitude, the system pressure increases as the wavelength increases.

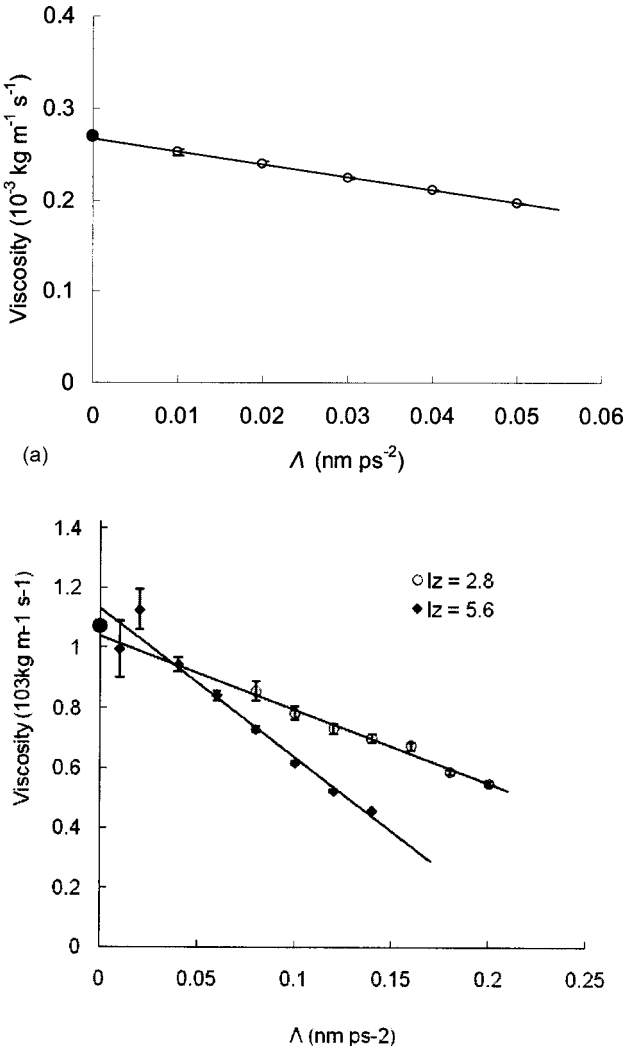

FIG. 2. The shear viscosity values of liquid argon at 86 K (a) and liquid ethanol at 298 K (b) predicted with various applied acceleration amplitudes (Λ). The shear viscosities of liquid ethanol (298 K) are calculated with two periodic wavelengths l_z (nm). The experimental values are denoted by black dots on the y axis.

It has been suggested that the maximum shear rate, which is the derivative of the generated velocity with respect to the z-coordinate,

$$s_{\max} = \max_z \left| \frac{\partial v_x(z)}{\partial z} \right| = \Lambda \frac{\rho}{\eta k}, \tag{14}$$

should be used to evaluate the perturbation strength.[10] However, the maximum shear rate is not known until the apparent viscosity η is known. A close analysis of our simulation data indicates that the ratio of the applied acceleration amplitude and the k-vector value measures the deviation of the system pressure. Therefore, we defined the perturbation index

TABLE III. The perturbation index χ ($nm^2\ ps^{-2}$), applied acceleration amplitude Λ ($nm\ ps^{-2}$), periodic perturbation vector k (nm^{-1}), maximum shear rate S_{max}(ps^{-1}), calculated average pressure (bar), and viscosity values η (10^{-3} $kg\ m^{-1}\ s^{-1}$) of liquid ethanol. The data are based on NVT ensemble simulations.

χ	Λ	k	s_{max}	P	η
0.03565	0.08	2.244	0.033	−10.720	0.857
	0.04	1.122	0.030	18.580	0.945
0.05348	0.12	2.244	0.058	85.640	0.730
	0.06	1.122	0.050	89.870	0.841
0.07130	0.16	2.244	0.083	187.440	0.672
	0.08	1.122	0.077	195.640	0.728
0.08913	0.20	2.244	0.128	362.990	0.549
	0.10	1.122	0.114	357.24	0.617

$$\chi = \frac{\Lambda}{k} \tag{15}$$

to measure the strength of the perturbation.

As given in Table III, the perturbation indexes calculated with different combinations of the amplitude Λ and k values correspond to roughly the same maximum shear rates and system pressures. In addition, examination of data in Table III indicates that with the perturbation indexes χ fixed, a smaller k-vector value indeed corresponds to a higher (and more accurate) apparent viscosity.

B. The origin of the underestimates

In order to understand why the predictions are generally underestimated at a given strength of the perturbation, we first analyzed the temperature distributions in the simulation boxes. Although the velocity profile was coupled to the heat bath and the velocity profile was excluded from the kinetic energy in the simulation,[10] the velocity profile generated by the applied external force should be associated with a temperature profile. To calculate the temperature profile, we divided the simulation box into 40 slabs in the z-direction and calculated the velocity in each of the slabs:

$$u_i = \left\langle \frac{\sum_{\text{slab}} m_j v_{xj}}{\sum_{\text{slab}} m_j} \right\rangle, \tag{16}$$

where m_j and v_{xj} are the mass and x (the direction of the applied force) component of the velocity of atom j in slab i. The velocity profiles of liquid ethanol calculated using different perturbation indexes are plotted in Fig. 3. The corresponding excess kinetic energy in the x-direction can be calculated:

$$\mathrm{KE}_i = \frac{1}{2}\left\langle \frac{(\sum_{\text{slab}} m_j v_{xj})^2}{\sum_{\text{slab}} m_j} \right\rangle. \tag{17}$$

The excess kinetic energy profiles of liquid argon and liquid ethanol with different perturbation index χ values are plotted in Fig. 4. The excess kinetic energy profile has the feature of the square of the velocity profile. Associated with the excess kinetic energy, the excess temperature profiles are plotted in Fig. 5. It is clear that there is a periodic temperature distribution in the z-direction. However, the difference in the tem-

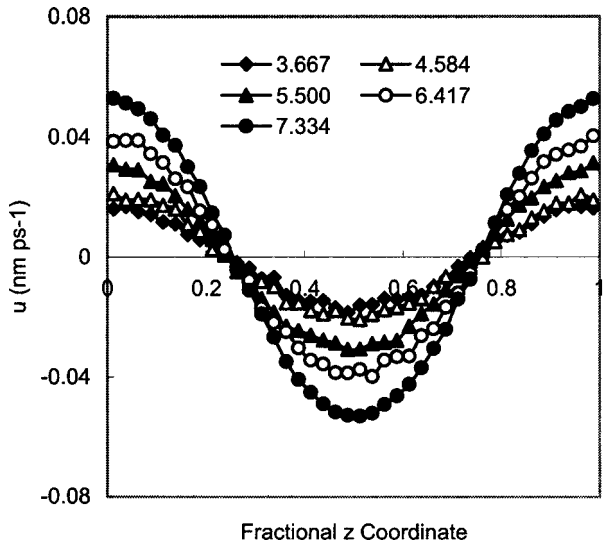

FIG. 3. Velocity ($nm\ ps^{-1}$) profiles of liquid ethanol as functions of various perturbation index χ (10^{-2} $nm^2\ ps^{-2}$).

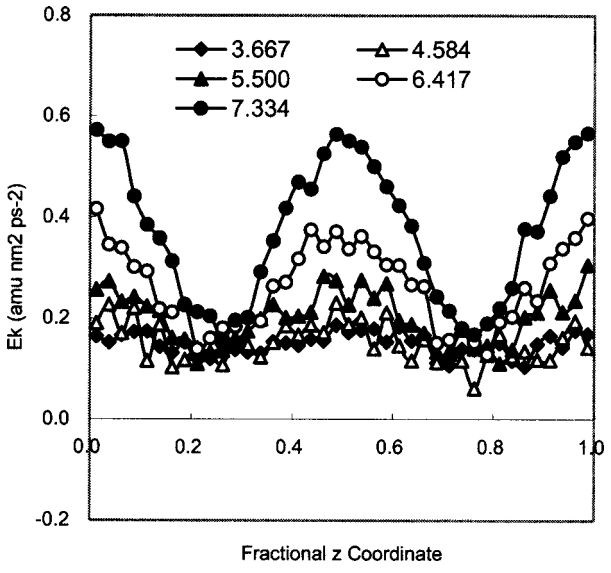

FIG. 4. Excess kinetic energy (amu $nm^2\ ps^{-2}$) profiles of liquid ethanol as functions of various perturbation index χ (10^{-2} $nm^2\ ps^{-2}$).

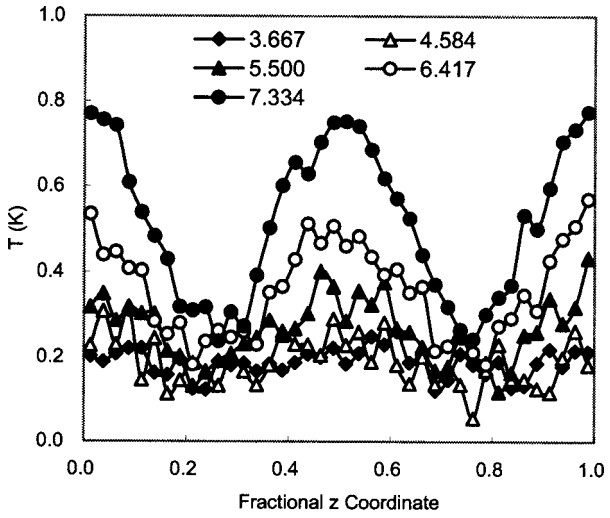

FIG. 5. Excess temperature profiles (k) of liquid ethanol as functions of various perturbation index χ (10^{-2} nm^2 ps^{-2}).

perature along the z-direction is insignificant. The differences between the maximum and minimum temperatures are less than 0.8 K as given in Fig. 5.

We further investigated the internal stress caused by the applied perturbation forces. This was done using the NPT ensemble simulation in which the total pressure is coupled with a "pressure bath," but the pressure tensors are anisotropic due to the applied external forces. In Table IV the pressure tensors of liquid ethanol with various perturbation indices are listed. The pressure tensors are negative in the x-direction (the direction of the external force), positive in the z-direction, and relatively stable in the y-direction. The pattern is consistent as the perturbation strength changes.

The phenomenon observed in the pressure tensors can be understood by considering how the non-ideal pressure is calculated:

$$P_{ss} = -\frac{1}{3V}\left\langle \sum s\frac{\partial U}{\partial s}\right\rangle, \tag{18}$$

where s denotes a specific coordination component. As the external force with gradient in the z-direction is applied, a continuum body is stretched in the x-direction, contracted in the z-direction, and steady in the y-direction, as illustrated in Fig. 6. At the microscopic level, the average intermolecular distances are stretched in the x-direction. The internal force $\partial U/\partial x$, which is a counter force of the external one, is in the same sign as the x-coordinate. Therefore, the pressure is

TABLE IV. The perturbation index χ (10^{-2} nm^2 ps^{-2}), average pressures P (bar), and pressure tensor diagonal components P_{xx}, P_{yy}, and P_{zz} (in bar) of liquid ethanol. The data are based on NPT ensemble simulations.

χ	P	P_{xx}	P_{yy}	P_{zz}
0.0	1.14	1.93	−1.41	2.88
3.66	1.36	−4.91	0.90	8.07
4.57	0.90	−27.38	12.60	17.47
5.49	1.06	−20.91	2.09	22.02
6.40	1.02	−41.13	12.67	31.51
7.32	0.82	−52.91	10.34	45.01

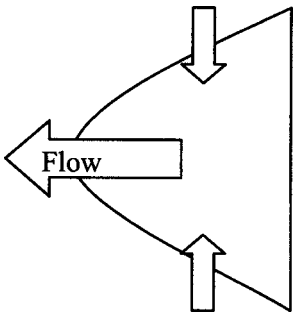

FIG. 6. As the external force applied to the continuum fluid causes a flow, the body of fluid is stretched in the direction of the flow and squeezed in the directions normal to the flow.

negative. In the z-direction, the average distance between molecules is compressed. The counter force $\partial U/\partial z$ is in the opposite direction of the z-coordinate; the contribution to pressure tensor is therefore positive. The pressure tensor in the y-direction does not change significantly because there is no external force applied in this direction.

Finally, we examined the distribution of density. With different perturbation indexes, the number density profiles of liquid argon and ethanol were calculated. The results are displayed in Fig. 7. Comparison of Fig. 7 with Figs. 5 and 6 shows that the number densities are correlated with the ki-

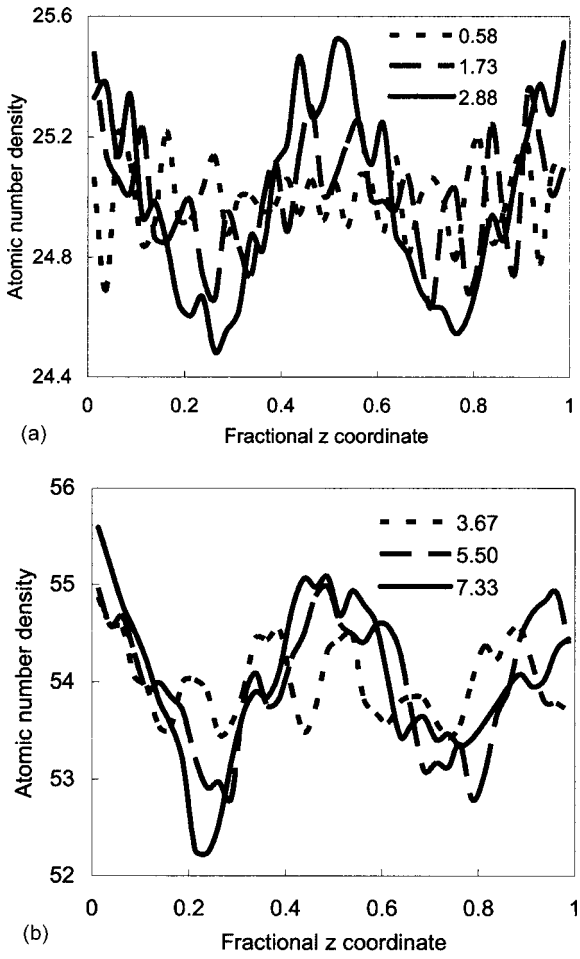

FIG. 7. The number density profiles of liquid argon (a) and liquid ethanol (b) as functions of various perturbation index χ (10^{-2} nm^2 ps^{-2}).

TABLE V. Comparison of calculated and experimental viscosities (10^{-3} kg m^{-1} s^{-1}) using the OPLS force field.

Liquid	Calculated	Experimental	Δ (%)
Propene	0.277	0.270	2.6
n-pentane	0.305	0.283	7.8
Ether	0.380	0.295	28.8
Ethylacetate	0.428	0.439	−2.5
Butane	0.432	0.360	20.0
Heptane	0.437	0.369	18.4
Isobutane	0.497	0.399	24.6
Acetone	0.501	0.305	64.4
Benzene	0.600	0.602	−0.3
Toluene	0.653	0.550	18.7
Decane	0.780	0.910	−14.3
Cyclohexane	1.062	0.895	18.7
Cresol	1.579	1.900	−16.9
Formic acid	1.799	1.510	19.1
n-hexane	0.332	0.315	5.4
Ethanol	1.040	1.074	−3.2

netic energy and temperature profiles. The high kinetic energy and temperature correspond to high number density. Moreover, the fluctuation in the density profile is perceptible even with the weakest perturbation.

As shown in Fig. 7, the maximum differences between the high and low densities are roughly 3%–5% of the number densities. The fluctuation is significant for apparent viscosity if it were viewed as a result of the thermal expansion. For example, a 5% change in density for water corresponds to a temperature change of 100 K (from 273 to 373 K); similarly, it corresponds to 7 K and 40 K changes in temperature for argon and ethanol liquids, respectively. The system can be viewed as slides of masses with different densities moving with different speeds. At the low density region (where the velocity is low) the intermolecular interactions are weaker than those at the high density region (the mass moves faster). The low density region makes the high-density region slippery, which leads to the underestimate of the viscosity. The gradients of the density profiles are associated with the perturbation index. However, as we have demonstrated, it does not vanish unless the perturbation is completely stopped. Therefore, the calculated viscosity is always lower than the true value.

C. The impact of force field quality

Because the apparent viscosity is always underestimated and linearly correlated with the applied external force, a linear extrapolation scheme can be used to predict the true shear viscosity. The shear viscosity of 16 molecular liquids predicted using this method and the OPLS force field[13] are compared with the experimental data[20] in Table V. The force field was derived based on the equilibrium data (heat of vaporization and density). Without any modification, the force field appears to be able to predict the transport properties with reasonable success. Most predictions are within 20% errors from the experimental data, which are similar to those reported for alkane liquids in the literature.[21,22] However, a few errors in Table V are above 20%. Although the low errors are mostly associated with nonpolar molecules, the predicted value for liquid ethanol is in excellent agreement (−3.2%) with the experimental data. Therefore, the errors are likely associated with the quality of the force field.

An exceptionally large error (64.4%) is associated with liquid acetone as given in Table V. The predicted heat of vaporization and equilibrium density of liquid acetone are in reasonable agreement with the experimental data using the OPLS force field.[13] However, a close examination of the force field parameters reveals that the atom types of the methyl group in acetone are the same as those in the alkane molecules. Consequently, the atomic partial charges used in the default OPLS force field are the same as those used in the alkanes, which are significantly different from that obtained by fitting the *ab initio* electrostatic potentials.

Therefore, we reparameterized the parameters for acetone. The parameterization procedure has been reported in previous publications.[23,24] The valence parameters were derived by fitting the energy data of the molecule calculated at the B3LYP/6–31 g(d) level. The charge parameters were derived by fitting the electrostatic potentials. Since the properties of liquids are the major concern, the polarizable continuum solvent model (PCM) (Ref. 25) was employed to calculate the charge parameters. The molecular dipole moment obtained using the *ab initio* charge parameters is 3.45 D, which is about 11% larger than that calculated using the OPLS charge parameters. With the valence and charge parameters fixed, the Lennard-Jones parameters originally taken from the OPLS force field were optimized by manually fitting the liquid density and the heat of vaporization of liquid acetone at 298 K. The derived parameters are listed in Table VI. With the optimized parameters the simulated liquid density and heat of vaporization at 298 K are 788 kg m^{-3} and 31.84 kJ mol^{-1}, in excellent agreement with the experimental data of 784 kg m^{-3} and 31.88 kJ mol^{-1}, respectively.

The predicted shear viscosities using the newly derived parameters are plotted in Fig. 8. The result calculated using default OPLS parameters and the experimental data are also labeled in the figure for comparison. The new prediction, 0.3436×10^{-3} kg m^{-1} s^{-1}, is only 7.4% higher than the experimental value of 0.32×10^{-3} kg m^{-1} s^{-1}, significantly better than that predicted using the original OPLS parameters. It should be emphasized that the new predictions were based on the parameters optimized using the equilibrium properties without any consideration of the transport properties. It demonstrates that a high-quality force field that parameterized using the *ab initio* data and the equilibrium properties of fluid can be used to predict the shear viscosity reliably.

IV. CONCLUSION

The application of the periodic perturbation method (PPM) was studied systematically in this work. Although the periodic wave-vector (k) should be small in order to satisfy the Navier-Stokes equation as suggested in the literature, we found a smaller k value leads to larger perturbation when the applied acceleration amplitude is fixed. Therefore, it could be misleading if only the selection of k value is emphasized. By

TABLE VI. Optimized force field parameters of acetone; the definition of the atom types is the same as that used in the OPLS force field.

Nonbond terms					$q(e)$	σ(nm)	ε(kJ mol^{-1})
CT					−0.378	0.34465	0.22092
HC					0.106	0.23856	0.10042
C_2					0.683	0.36922	0.35187
O_2					−0.563	0.29116	0.70500
	Bond terms					b_0(nm)	k(kJ nm^{-2})
CT	HC					0.10982	304950.7
C_2	CT					0.15542	177787.6
C_2	O_2					0.12207	745425.3
	Angle terms					a_0(°)	k(kJ rad^{-2})
CT	C_2	O_2				120.865	653.912
CT	C_2	CT				117.355	129.156
C_2	CT	HC				108.307	390.034
HC	CT	HC				103.969	296.43
Dihedral terms (kJ mol^{-1})				c_1	c_2	c_3	c_4
CT	C_2	CT	HC	18.626	1.845	−18.011	−2.46
HC	CT	C_2	O_2	−0.148	0.354	0.266	−0.472
	Improper dihedral terms			φ(°)	k(kJ mol^{-1})	N	
CT	CT	C_2	O_2	180	80.75	2	

defining a perturbation index which is a quantity of the applied acceleration amplitude divided by the periodic wavevector value (k) we found the extent of perturbation can be accurately measured before the simulation is done.

Application of PPM to 16 representative organic liquids shows that apparent viscosities are always underestimated. The origin of the underestimates has been systematically analyzed. The applied periodic force causes a periodic profile in velocity, which leads to periodic distributions of kinetic energy and temperature. However, the fluctuation in temperature is negligible for causing the viscosity changes at normal condition. The variation in velocity causes anisotropic distribution of the pressure tensors in the system. This phenomenon is analog to the Bernoulli phenomenon of moving fluid. Consequently, there is a periodic distribution of liquid density in the simulation box. The liquid density is higher in the region where the mass moves faster. The density profile is acoustic, with the wavelength of the half of the cell edge in phase with the distribution of the kinetic energy and temperature. The fluctuation of density is significant with typical values of 3%–5% of the total density. It is the uneven density profile that causes the reduction of the apparent viscosity.

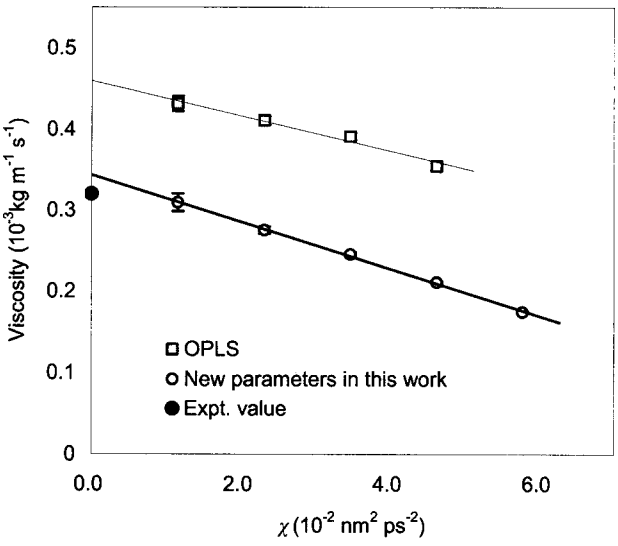

FIG. 8. The shear viscosities of acetone liquid calculated with default OPLS force field and the newly derived force field in this work. The experimental data are denoted by a dot on the y axis.

The perturbation cannot be completely removed unless the applied force is completely removed. This is unlike the phenomenon reported in the literature using other NEMD methods such as SLLOD in which the Couette flow is simulated by applying a linear velocity (constant gradient) in the z-direction and a Newtonian fluid can be obtained by reducing the applied velocity below a certain threshold. In the PPM, it appears the periodic gradient in the applied acceleration makes the uneven distribution persistent even at very small external forces. However, the predictions of viscosities are linearly responsible to the applied forces, therefore, a linear extrapolation can be used to get the "nonperturbed" viscosity consistently. This makes the PPM prediction reliable, at least for small molecular liquids.

Force field is an important factor affecting the predictions. The force field derived using *ab initio* and equilibrium properties can be used to predict the transport properties with reasonable accuracy. It appears that if the parameters are derived using high quality of *ab initio* data, and optimized using the heat of vaporization and liquid density, the relative

errors in the calculated viscosity using the extrapolation protocol are less than 10%.

ACKNOWLEDGMENTS

Financial support from the National Science Foundation of China (Grant No. 10676021) and National Basic Research Program of China (Grant Nos. 2003CB615804 and 2007CB209700) is gratefully acknowledged.

[1] J. P. Hansen and I. R. McDonald, *Theory of Simple Liquids*, 2nd ed. (Academic, London, 1986), pp. 267–278.
[2] B. J. Palmer, Phys. Rev. E **49**, 359 (1994).
[3] D. J. Evans and G. P. Morriss, *Statistical Mechanics of Nonequilibrium Liquids* (Academic, London, 1990), pp. 1–4.
[4] D. J. Evans and G. P. Morriss, Phys. Rev. A **30**, 1528 (1984).
[5] E. M. Gosling, I. R. McDonald, and K. Singer, Mol. Phys. **26**, 1475 (1973).
[6] G. Ciccotti, G. Jacucci, and I. R. McDonald, Phys. Rev. A **13**, 426 (1976).
[7] F. Müller-Plathe, Phys. Rev. E **59**, 4894 (1999).
[8] G. Arya, E. J. Maginn, and H. Chang, J. Chem. Phys. **113**, 2079 (2000).
[9] V. R. Vasquez, E. A. Macedo, and M. S. Zabaloy, Int. J. Thermophys. **25**, 1799 (2004).
[10] B. Hess, J. Chem. Phys. **116**, 209 (2002).
[11] E. J. W. Wensink, A. C. Hoffmann, P. J. van Maaren, and D. van der Spoel, J. Chem. Phys. **119**, 7308 (2003).
[12] L. Zhao, X. Wang, L. Wang, and H. Sun, Fluid Phase Equilib. **260**, 212 (2007).
[13] W. L. Jorgensen, D. S. Maxwell, and J. Tirado-Rives, J. Am. Chem. Soc. **118**, 11225 (1996).
[14] H. Flyvbjerg and H. G. Petersen, J. Chem. Phys. **91**, 461 (1989).
[15] L. Verlet and J. Weis, Mol. Phys. **24**, 1013 (1972).
[16] D. van der Spoel, E. Lindahl, B. Hess, G. Groenhof, A. E. Mark, and H. J. Berendsen, J. Comput. Chem. **26**, 1701 (2005).
[17] S. K. Sinha, *Physics of Particles, Nuclei and Materials: Recent Trends*, edited by R. K. Gupta (Narosa, Delhi, 2002), p. 248.
[18] M. P. Allen and D. J. Tildesley, *Computer Simulations of Liquids* (Clarendon, Oxford, 1987).
[19] B. A. Younglove and H. J. M. Hanley, J. Phys. Chem. Ref. Data **15**, 1323 (1986).
[20] *Chemical Properties Handbook*, edited by C. L. Yaws (McGraw-Hill, New York, 1999).
[21] W. Allen and R. L. Rowley, J. Chem. Phys. **106**, 10273 (1997).
[22] N. G. Fuller and R. L. Rowley, Int. J. Thermophys. **21**, 45 (2000).
[23] H. Sun, J. Phys. Chem. B **102**, 7338 (1998).
[24] J. Dai, C. Wu, X. Bao, and H. Sun, Fluid Phase Equilib. **236**, 78 (2005).
[25] B. Mennucci and J. Tomasi, J. Chem. Phys. **106**, 5151 (1997).